Physics Open 23 (2025) 100259

Contents lists available at ScienceDirect

Physics Open

journal homepage: www.sciencedirect.com/journal/physics-open

Excellent self-assembly properties of Iron Phthalocyanines on alumina for locally ordered single-atom catalysts

Fatema Mohamed [a,b,c,1], Manuel Corva [a,d,2], Erika Tomsič [a,3], Zhijing Feng [a,d,4], Tomáš Skála [e], Giovanni Comelli [a,d], Nicola Seriani [b], Erik Vesselli [a,d], Maria Peressi [a,*]

[a] Physics Department, University of Trieste, via A. Valerio 2, Trieste, 34127, Italy
[b] The Abdus Salam ICTP, Strada Costiera 11, Trieste, 34151, Italy
[c] Department of Physics, University of Khartoum, PO Box 321, Khartoum, 11115, Sudan
[d] CNR - Istituto Officina dei Materiali (IOM), S.S. 14 km 163.5, Area Science Park, Basovizza, Trieste, 34149, Italy
[e] Charles University, Faculty of Mathematics and Physics, V Holešovičkách 2, 18000 Prague 8, Czech Republic

A B S T R A C T

In a biomimetic approach, metal Phthalocyanines (Pcs) can be considered to efficiently model single atom catalysts (SACs), hosting catalytically active single metal atoms in their macrocyclic cages. An ordered 2D array of SACs can thus be obtained when metal Pcs are assembled in a regular framework. In this work we consider in particular Iron Pcs (FePcs) on an ultra-thin alumina film grown on the $Ni_3Al(111)$ surface. Intrinsic modulations in the potential energy surface related with the oxide film structure drive the self-assembly of FePc molecules into a regular array, with molecular vacancies forming a hexagonal Bravais lattice with the same periodicity of the substrate, i.e. with a lattice parameter of about 4 nm. The symmetry of the supramolecular structure is dictated by the template rather than by the C_{4v} symmetry of the individual molecules, thus indicating prevalence of molecule-substrate interactions with respect to intermolecular forces. The same hexagonal periodicity extends also to the multilayer, which starts forming already before completion of the first, interfacial monolayer. The latter exhibits a local definite chirality, also propagating to the multilayer in a determined stacking sequence.

1. Introduction

Phthalocyanines (Pcs) [1] are square planar organic molecules with chemical formula $C_{32}H_{18}N_8$ that consist of four isoindole units linked by nitrogen atoms. If the two hydrogen atoms in the central cavity of the molecule are replaced by a metal atom, the resulting compound is normally referred to as Metal Phthalocyanine (MPc, $MC_{32}H_{16}N_8$).

MPcs have a chemical and geometric structure closely resembling the porphyrinic pocket of biological macromolecules. Since their discovery in the early nineteens [2], Pcs have become a topic of interest for many experimental as well as theoretical scientists, aiming at understanding the detailed process of the catalytically active part in more complex biological molecules such as chlorophyll and hemoglobin. These molecules incorporate active centers in large organic superstructures and, as in many enzymes [3], the size of the catalytically active part is reduced to the extreme, basically to single metal atoms. The organic part instead usually handles the interaction with the surrounding molecular backbone, stabilizes the active site and contributes to the tuning of the electronic configuration of the metal atom. MPcs can mimic at a simplified level both the catalytic active part and the organic structure of biological systems, while they can also be used in a biomimetic approach to synthetize both model and applicative single atom catalysts (SACs) [4,5].

Not only as model systems, Pcs and MPcs are broadly investigated for their actual technological applicability as oxidation catalysts [6], organic light-emitting diodes [7], molecular organic photovoltaics [8–10], photosensitizers in dye solar cells [11], organic thin film transistors [12], electroreduction catalysts [13], and for many further applications. Among many heme-like molecules, the Iron Pc (FePc) is one of the most interesting species, since it was shown to act as a good catalyst in oxygen reduction reactions [14] and to efficiently adsorb and activate carbon dioxide [15].

This article is part of a special issue entitled: Advancements in Physics published in Physics Open.

* Corresponding author.
E-mail address: peressi@units.it (M. Peressi).

[1] Presently at: LSI, École Polytechnique, Institut Polytechnique de Paris, F-91120 Palaiseau, France.
[2] Presently at: Sensirion AG, Stäfa, Switzerland.
[3] Presently at: University of Nova Gorica, Slovenia.
[4] Presently at: Intel Corporation, Hillsboro, Oregon, United States of America.

https://doi.org/10.1016/j.physo.2025.100259
Received 30 December 2024; Received in revised form 6 February 2025; Accepted 21 February 2025
Available online 22 February 2025

Elucidating the behavior and self-assembly properties of metal-organic molecules on an appropriate support is pivotal for optimizing the stability, efficiency, and selectivity of their active centers. Furthermore, this understanding facilitates the organization of these molecules into locally ordered SACs, thereby addressing practical challenges of SAC-based systems such as low atom loading density and uncontrollable spatial distribution [16]. Indeed, charge transfer effects at the metal-organic/inorganic interface of a heterostack may be exploited to govern the properties of the layer, in a competition among lateral interactions, interactions with the support, and trans-effects [17–19]. On a low-interacting support such as monolayer graphene on Ir(111) MPcs generally form highly ordered, almost square lattices, but the symmetry of the substrate can play a role in the formation of supramolecular architectures. The self-assembly of various MPcs has been previously studied combining experimental surface science techniques like Scanning Tunneling Microscopy (STM) and *ab-initio* Density Functional Theory (DFT) calculations. These studies provide a comprehensive understanding of the structural properties of the molecule, adsorption sites, nature of bond, charge distribution between the molecules and the substrate, and interaction between the molecules [20]. In particular, the behavior of FePcs on different metal surfaces was studied by many authors [20–31].

Motivated by the relevance of FePcs, we devoted our attention to studying their self-assembly on a specific substrate, an ultra-thin alumina film (Al_2O_3) grown on the $Ni_3Al(111)$ surface. The deposition of different metals on this substrate has already been exploited for the creation of stable ordered arrays of metal nanoclusters, seeded by the "hole" sites of the film [32–34]. For what concerns MPcs, only the self-assembly of Cu(II)Pc molecules on this substrate was reported so far, showing no role of the surface template [35]. Instead, we found that the same $Al_2O_3/Ni_3Al(111)$ substrate plays a dominant role in the self-assembly of FePcs through a mechanism driven by a molecule–substrate interaction scheme that can be switched to a molecule–molecule driven regime by the pre-deposition of Cu clusters [36].

Complementing the results reported in Ref. [36], focused on the effect of metallic nanoparticles hosted on the alumina matrix on the self-assembly of a monolayer of adsorbed FePcs, we now shift our focus to the adsorption of FePcs on pristine $Al_2O_3/Ni_3Al(111)$ and their self-assembly driven by the molecule–substrate interaction. We thus emphasize the role of the substrate and extend the investigation from a metallorganic monolayer to a bilayer, discussing the structural details for both cases as well as the interlayer interaction within the bilayer.

2. Methods

2.1. Experiments

The $Ni_3Al(111)$ single crystal termination was cleaned by standard UHV sputtering–annealing cycles (Ar^+/Ne^+, 1170 K). Temperature was monitored by a K-type thermocouple. Following established recipes, controlled oxidation of the surface yields a high-quality ultra-thin alumina layer [37]. In detail, surface oxidation was accomplished through three annealing cycles at 1000 K in 2×10^{-7} mbar O_2 followed by UHV annealing at 1070 K. Molecular depositions were performed under UHV conditions with the oxide surface at room temperature. FePcs were purchased from TCI Europe with a purity above 98 % and sublimated from a heated quartz crucible. Depending on the setup, the coverage was estimated calibrating the evaporators by means of a quartz microbalance (STM) or through C 1*s* and Al 2*p* core level intensities (XPS).

XPS and STM experiments were performed under UHV conditions (low 10^{-10} mbar) at room temperature and LN_2 (77 K), respectively. Photoemission spectra were collected at the Materials Science Beamline end-station at the Elettra synchrotron facility through a Specs Phoibos 150 high-luminosity electron-energy analyzer. C and N 1*s* core level regions were measured at normal emission, selecting 400 and 500 eV incident photon energies, respectively, and normalized to the lower binding energy side background. The data were analyzed by least-square fitting with Voigt profiles, taking into account a linear background. STM measurements were carried out with an Omicron Low Temperature STM system in constant current mode, with the bias applied to the sample and a grounded W tip. Images were analyzed by subtracting a background plane and by applying an appropriate affine transformation to compensate for thermal-drift effects.

2.2. Theory

Spin-polarized ab-initio Density Functional Theory (DFT) calculations were carried out using the Quantum ESPRESSO [38] suite of codes, with ultrasoft pseudopotentials publicly available [39]. The semi-local Generalized Gradient Approximation (GGA-PBE) [40] for the exchange correlation functional have been used throughout, in addition to semi-empirical corrections accounting for Van der Waals interactions using the DFT-D approach [41].

The unit cell describing the aluminum oxide (Al_2O_3) grown on Ni_3Al (111) is hexagonal with in-plane lattice parameter of 41.5 Å (Fig. 1, left panel). Considering two layers of Ni_3Al under the Al_2O_3 thin film, the entire supercell contains 1257 atoms. The atomic coordinates are those obtained by Schmid et al. [42] and already used in Refs. [33,34,36]. The unit cell contains peculiar sites giving rise to two ordered superstructures. One peculiar site corresponds to a hole (oxygen vacancy, visible as a "hole" in the model of Fig. 1, left panel) reaching the metal substrate: it forms a so-called "dot" structure with the same periodicity of the oxide film. There are two additional high-symmetry sites per unit cell, at a distance of 24 Å one from each other, determining a so-called "network" structure (yellow triangles in the model of Fig. 1, left panel). These and other neighboring sites have been tested in Refs. [33,34] for the adsorption of different metal atoms.

To describe the adsorption of an individual FePc adsorbed on the substrate or the structure of a monolayer or multilayer FePc, proper reduced models have been used to decrease the computational effort, as specified in the following.

The adsorption of a single FePc on $Al_2O_3/Ni_3Al(111)$ substrate has been simulated with a cluster geometry, using a portion of the substrate cut from the entire unit cell in selected regions around the so-called "dot" or "hole" and around the "network" sites, without the full periodicity; such portions are indicated by the dashed yellow lines in the model of Fig. 1, left panel, and shown in the same figure in the central and right panels (see also the Results and Discussion section). A total of 385 atoms (205 atoms for the alloy and 180 atoms for the alumina) and 345 atoms (148 atoms for the alloy and 197 atoms for the alumina) surrounded by vacuum have been considered respectively around the "hole" and the "network" sites. These pieces of the substrate, with only one molecule adsorbed, were placed in a 31.02 Å × 31.02 Å × 26.07 Å hexagonal supercell, large enough to avoid interaction among the repeated images of the molecule. Full optimization of the molecular structures has been carried out, while keeping the substrate fixed.

The periodic hexagonal self-assembled FePc molecular layer was modelled using a hexagonal supercell with the same in-plane dimension of the oxide template (in-plane lattice parameter of 41.5 Å), as suggested from the inspection of the experimental STM images, and a perpendicular size of 26.07 Å, but without the substrate. The supercell describing a FePc monolayer contained 6 FePc molecules per cell. The molecules were fully relaxed, apart from the Fe atoms, which were kept fixed on a plane and whose in-plane positions were determined from experiments (the Fe atoms of the Pcs correspond to the positions of specific O-on top sites of the template). The supercell describing a FePc bilayer contained 12 molecules; the coordinates of the additional molecular layer have been fully optimized.

The plane wave basis set was truncated at a kinetic energy cutoff of 30 Ry (300 Ry for the charge density). The Methfessel–Paxton smearing technique with an energy broadening of 0.02 Ry was used [43]. Due to

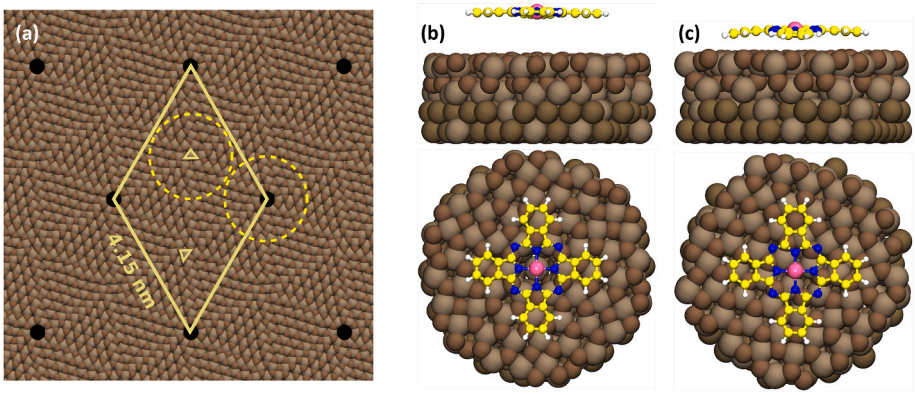

Fig. 1. Stick-and-ball models of the alumina substrate and of a single FePc adsorbed on different sites of the alumina ultra-thin film, with optimized positions obtained by DFT. (a): top view of the full model of the alumina substrate with the sketch of the unit cell (solid yellow line), the "network" sites (triangles), the portions cut around the "dot" and the "network" sites to build the reduced models (dashed yellow lines). (b): FePc on the "dot" region, corresponding to an oxygen vacancy; (c): FePc on the "network" region. In panels (b) and (c), side/top views are reported in the top/bottom images, respectively. Oxygen atoms are represented by smaller darker brown balls.

the large cells size, only the Gamma point was used for the Brillouin zone integration. Ionic coordinates were optimized until the total forces were smaller than 0.03 eV/Å^{-1}.

The adsorption energy of a molecule on the substrate was calculated as: $E_{ads} = E_{tot}$-E_M-$E_{substrate}$, where E_{tot} is the total energy of the system, E_M of a freestanding molecule, and $E_{substrate}$ of the substrate. The lateral interaction in the FePc monolayer has been calculated by subtracting E_M from the total energy of the hexagonal unit cell of the monolayer divided by six to be normalized to one molecule.

The STM images were simulated using the Tersoff–Hamman approach, where the energy-integrated electronic local density of states (ILDOS) is proportional to the tunneling current [44]. In particular, isosurfaces of ILDOS were mapped in order to simulated constant-current STM images.

In order to confirm the reliability of our GGA-PBE results in presence of *d* electronic states in the Fe pseudopotential, we also performed some GGA + U calculations [45] and checked the effect of Hubbard correction on the energetics and electronic properties. The "+U" correction, fixed at +1 eV [36] had pronounced effects on the electronic structure around the Fermi energy and consequently on the bias at which some specific bright features appeared in the simulated STM images, but no appreciable effect on the equilibrium structures and adsorption and interaction energies. Therefore, only GGA-PBE results are reported in this work.

3. Results and discussion

3.1. Single FePc molecule

The structure of a thin film of aluminum oxide (Al_2O_3) grown on $Ni_3Al(111)$ was previously determined by combining DFT calculations with AFM and STM experiments [42,46]. As already mentioned in the Methods section, we have investigated by DFT the adsorption of an individual FePc centered on the "dot" and "network" sites using reduced models. We found that the most stable adsorption configuration for the FePc is in the "network" region with Fe on top of an O atom. This configuration is the most stable of three possible different combinations (bridge, hollow and O-top) and in analogy to the case of many single metal atoms on this alumina layer [32,34]. This configuration is also much more stable than the adsorption on the hole site: the molecule therefore avoids adsorbing at the holes. The adsorption energies on top of an O atom in the "network" region and on top of a hole are 2.76 eV and 0.61 eV, respectively. The top and side views of the corresponding DFT optimized stick-and-ball models are presented in Fig. 1. In both regions the molecule is adsorbed parallel to the substrate, but on the most stable adsorption site it is slightly distorted, with the peripheral moieties slightly bent toward the substrate. The difference between the z coordinate of the H atoms in the pyrroles and the Fe atom ranges from 0.32 Å to 0.73 Å, indicating a configuration that is not perfectly symmetric because of the different local registry of parts of the molecule with the underlying substrate. In the "network" region, the distance of the molecule from the oxide surface is on average 3.02 Å, and 3.27 Å for the Fe atom, to be qualitatively compared with the apparent height of 2.6 ± 0.3 Å reported in Ref. [32] for a single Fe atom at the same site.

Conversely, the average molecule–surface distance on the "hole" is 5.53 Å. The magnetic moment of the FePc is 2.25 μ_B/cell for both configurations, with an increase of 0.24 μ_B/cell with respect to the freestanding molecule, presenting a fully planar structure with a total magnetic moment of 2.01 μ_B/cell, in accordance with previous results obtained with the same functional [29]. This similarity indicates a weak molecule-substrate interaction and foresees a weak surface trans-effect. The simulated STM images at different bias voltage for the molecule adsorbed on the "network" region are reported in Ref. [36] and compared with the experimental images, showing an excellent matching.

3.2. FePc monolayer

In a previous work we investigated the distribution of FePcs on the $Al_2O_3/Ni_3Al(111)$ surface with and without decorating it with Cu nanoclusters [36]. We focused on relatively low FePcs coverage (referred to the Ni_3Al termination), showing that the molecules locally arrange in different single-layer structures depending on the surface pre-treatment. In the following, we recall our most relevant findings and report new details about their self-assembly on the bare alumina termination at higher molecular loadings.

Fig. 2 shows a STM images of FePc molecules on alumina at a coverage that does not allow full completion of the monolayer. Nevertheless, most of FePcs are arranged in a locally ordered self-assembled structure, and only a few molecules are isolated, in pairs or in small, aggregated islands. This suggests the presence of attractive, but not dominating, lateral molecule-molecule interactions. In contrast with the almost square superstructure adopted on the same substrate with predeposition of Cu clusters [36] (and on other substrates, as reported in Ref. [20]), this ordered structure is characterized by the same unit cell of the underlying alumina template, resulting in regular patterns of FePcs and FePc vacancies. The region reported in Fig. 2 presents a molecular superstructure with a well-defined chirality, but domains with supramolecular structure of opposite chirality coexist in the system. An accurate analysis of the experimental STM images indicates that the molecular vacancies of the monolayer correspond to the oxygen

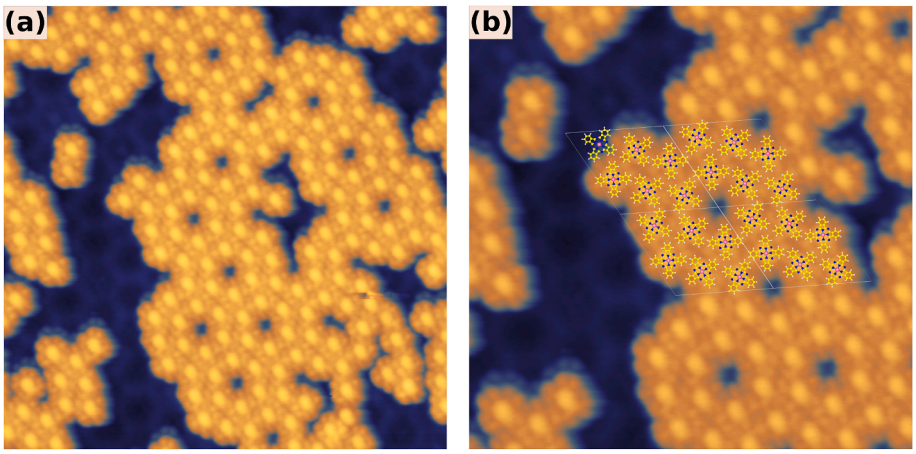

Fig. 2. Constant current STM images of FePc molecules self-assembled in a locally ordered hexagonal pattern on $Al_2O_3/Ni_3Al(111)$ support at low coverage (the contrast suggests that only one FePc monolayer has been deposited). In the zoomed region on the right, the stick-and-ball model of FePc molecular layer obtained by DFT simulations is superimposed to the STM images. Bias: +2.0 V; current: 5 pA; dimensions: 30 × 30 nm^2 for the left panel, 19 × 19 nm^2 for the right panel.

vacancies in the alumina layer, in agreement with our DFT predictions suggesting that FePcs avoid sitting on top of the oxygen vacancies.

Close inspection of the experimental STM images, with particular attention to the symmetry of the ordered pattern, suggests a structural model for the monolayer. In Ref. [36] we reported the DFT optimized hexagonal unit cell with six equivalent adsorption sites. On these, the molecules adsorb with an ordered pattern and a mutual orientation that are not related to their four-fold symmetry. Fig. 3 shows the FePcs arrangement around a molecular vacancy (cut in panel a), reporting experimental (a) and simulated (c) STM images, together with the DFT-optimized model (b). In Fig. 4 we compare the models for opposite chirality, obtained by simply mirroring the image. The height profile in the first panel of Fig. 3 (derived from the experimental STM image) is compatible with a central depression of about 4 Å, corresponding to the molecular vacancy, and a distance of 3.1 nm between opposite molecular centers across the vacancy. The optimized DFT model, where the molecules can freely adjust their orientation around the Fe centers, gives a mutual minimum distance of 2.10 Å between two closer H atoms and a mutual weak attraction with energy of 0.08 eV per molecule, much smaller than the molecule-substrate interaction (confirming the experimental interpretation). In conclusion, the FePcs self-assembly on the substrate and form a hexagonal superstructure driven by the molecule–substrate interactions and by weaker attractive molecule–molecule interactions. We observe that long-range order is not achieved, not even at higher coverage, while the growth of multilayers starts before completion of the monolayer. A similar behaviour was observed also in the case of CuPcs on the same substrate [35].

We have investigated the FePc monolayer adsorbed on the ultrathin alumina film also by means of X-Ray Photoelectron Spectroscopy (XPS). In Fig. 5 we plot the N and C 1*s* core level spectra collected at room temperature (left and right panels, respectively). As already observed for FePcs adsorbed on several substrates, the fitting of the N *1s* spectrum reveals two features centered at about 399 eV, associated with the two (generally unresolved) non-equivalent nitrogen atoms in the tetrapyrrolic ring ([36] and references therein). The corresponding C 1*s* spectrum (right) reveals instead two main adiabatic peaks due to the carbon atoms forming the benzenic (B) and pyrrolic (P) groups, respectively, and an additional feature ascribed to inelastic shake-up effects (S). By means of XPS we investigated also the stability of the adlayer. In the inset of Fig. 5 we plot the evolution of the core level intensities and of the core level shifts for both N and C 1*s* signals as a function of the (stepwise) annealing temperature. Drastic modifications are observed already above 450 K, yielding a shift of the spectral components of more than −300 meV, associated with a signal decrease of more than 40 % beyond 600 K. Based on the spectroscopic information, we can conclude that desorption and partial decomposition of the FePcs occur already upon mild heating of the layer, thus indicating a relatively poor temperature stability. However, the FePc metallorganic layer is strongly stabilized with respect to the CuPc case, where complete desorption occurs already after annealing to 350 K [35].

3.3. FePc bilayer

Fig. 6 shows experimental STM images of regions where FePc bilayers are present. The layer closer to the surface has an intermediate brightness (light blue) and can be clearly distinguished from the substrate (dark blue) and the second layer (yellow palette). The multilayer growth is strongly dependent on the ordering of the first molecular layer. The second molecular plane has the same structure and unit cell of the first one, and closer inspection indicates that the molecular

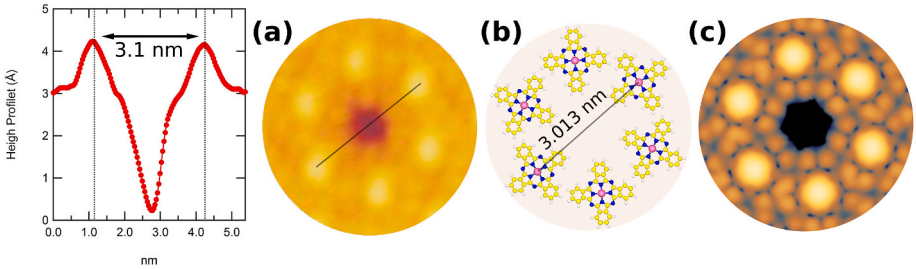

Fig. 3. FePc molecules self-assembled in a locally ordered hexagonal pattern around the "dot" site (oxygen vacancy) of the $Al_2O_3/Ni_3Al(111)$ support taken in a monolayer region. From left to right: height profile; experimental STM image at bias = +2 V; stick-and-ball model with optimized positions obtained by DFT; simulated STM image at the same bias.

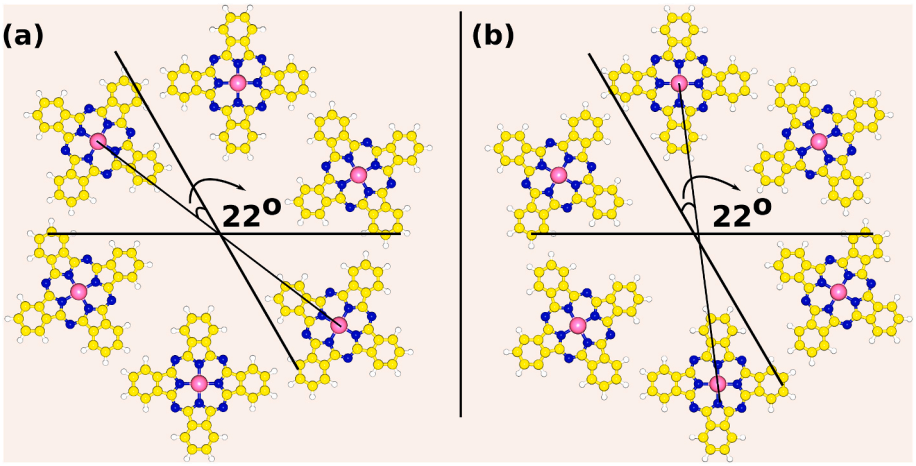

Fig. 4. Two stick-and-ball models of FePc molecules self-assembled in the ordered hexagonal pattern around the "dot" site (oxygen vacancy). The two structures are the same but have opposite chirality. The thicker solid lines sketch adjacent unit cells and the mirror axis of the structure, while the thinner line joining two Fe atoms is a guide to the eye to recognize the opposite chirality.

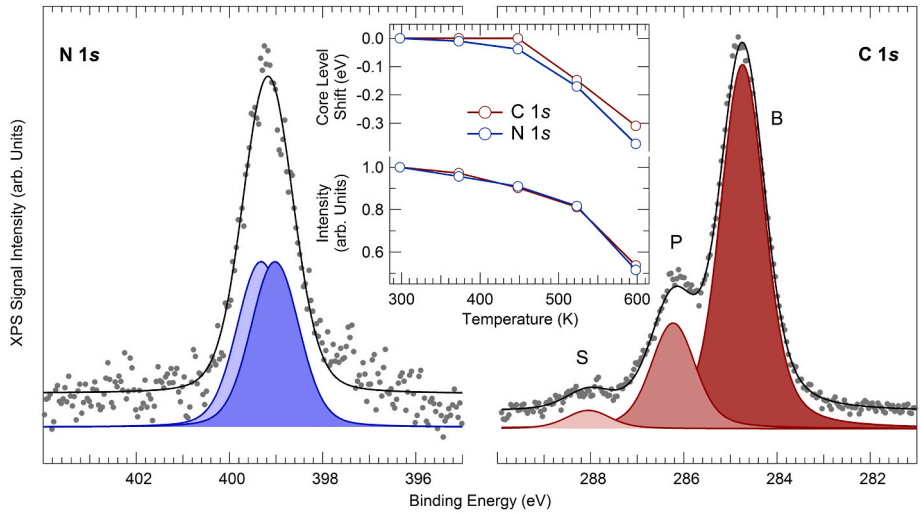

Fig. 5. N (left panel) and C (right panel) 1s core level spectra collected at room temperature upon deposition of FePcs on the ultrathin alumina film termination; data (grey dots) are shown together with the best fit sum (black lines) and with fitted into the separate spectral components (color filled profiles). The temperature dependence of the normalized core level signal intensities (bottom) and of the relative core level shifts (top) is shown in the inset.

vacancies are one on top of the other. This is in contrast with the CuPcs case on the same substrate, where the second layer was randomly oriented with respect to the first one [35]. The second layer of FePcs could possess the same or opposite chirality of the underlying layer (see the models in Fig. 4, where the opposite chirality can be recognized in the molecular arrangements around the "hole"). To clarify the peculiar chirality property of the bilayer, in Fig. 7 we report the results of our investigation of two different possible bilayer arrangements, one with a "face-to-back" (same chirality, one layer exactly on top of the other) and the other with a "face-to-face" stacking (opposite chirality, one layer flipped with respect to the other). DFT calculations performed for the two models shed light on the chirality of the bilayers: the most stable configuration indeed corresponds to the second case, with an attractive interlayer energy of 0.77 eV per molecule and an average interlayer distance of 2.98 Å, to be compared with 2.3 Å from the height profile obtained by the STM measurements (Fig. 8a). In the case of stacking with the same chirality, instead, there is a remarkable repulsive energy of −4.11 eV per molecule. For comparison, the interlayer distance was 3.5 Å for the case of CuPcs on the same template [35]. Fig. 8 shows also a zoom of the experimental (b) and of the simulated (d) STM images around the hole for the most stable DFT structure, together with its stick and ball model (c): the agreement is excellent, at variance with the simulated image for the face-to-back stacking (e).

4. Conclusions

In this work we have studied by means of a joint experimental and theoretical/computational investigation the excellent self-assembly capability of FePc molecules on an ordered template. We have shown how the self-assembly of FePcs on an ultrathin alumina film obtained by oxidation of the $Ni_3Al(111)$ termination is driven by the substrate rather than by intermolecular lateral interactions. The hexagonal periodicity of the self-assembled structure reflects that of the substrate, even in the coincidence with the vacancies, where a defect in the molecular layer corresponds to one in the substrate, suggesting a feasible route to build a locally ordered, patterned Fe SACs.

Interestingly, the substrate templating effect propagates into the structure of molecular multilayers. Finally, the ordered structure of FePcs presents domains with defined chirality. While these coexist in a single layer (which is not continuous even if the FePc saturation

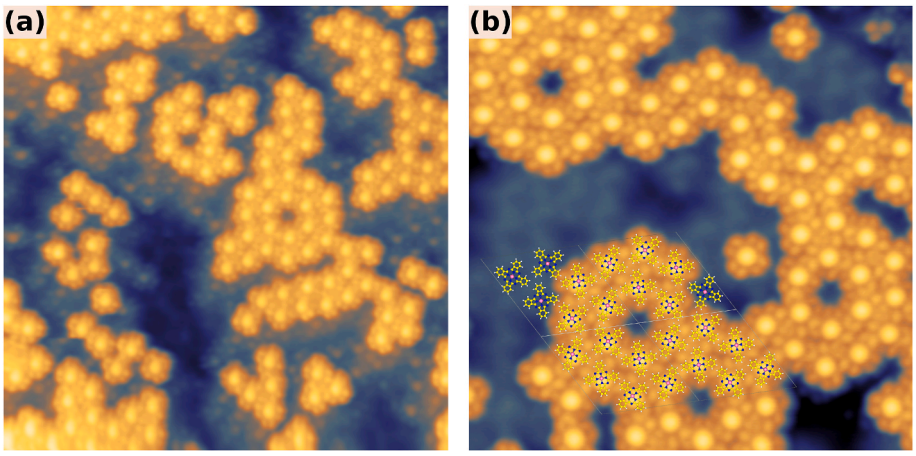

Fig. 6. Constant current STM images of FePc molecules self-assembled on $Al_2O_3/Ni_3Al(111)$ support at high coverage; the different contrast indicates regions with a monolayer (intermediate brightness) and a bilayer (brightest) of FePc molecules. In the zoomed region on the right, the stick-and-ball model of the uppermost FePc molecular layer obtained by DFT simulations is superimposed to the STM images, flipped with respect to the right panel of Fig. 2. Bias: +2.0 V; current: 5 pA; dimensions: 30 × 30 nm^2 for the left panel, 19 × 19 nm^2 for the right panel.

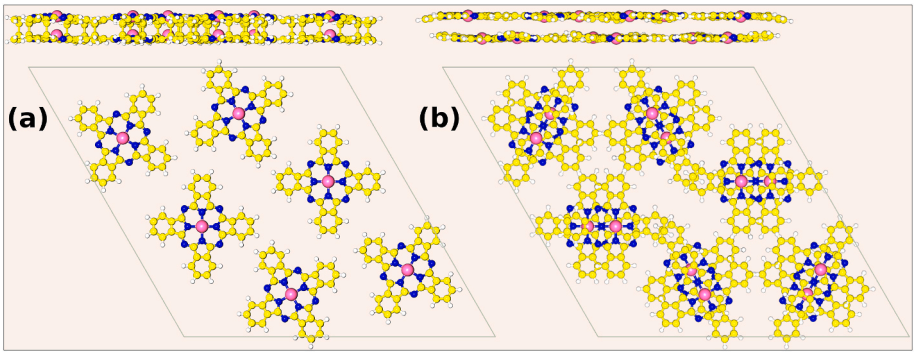

Fig. 7. Stick-and-ball models of a FePcs bilayer. With reference to the possibility of opposite chirality of the hexagonal self-assembled monolayer, the model (a) represents a back-to-face superposition (vertical stacking without change of chirality, with one layer exactly on top of the other) and the model (b) a face-to-face stacking, with a change of chirality. Side/top views in the upper/lower panels.

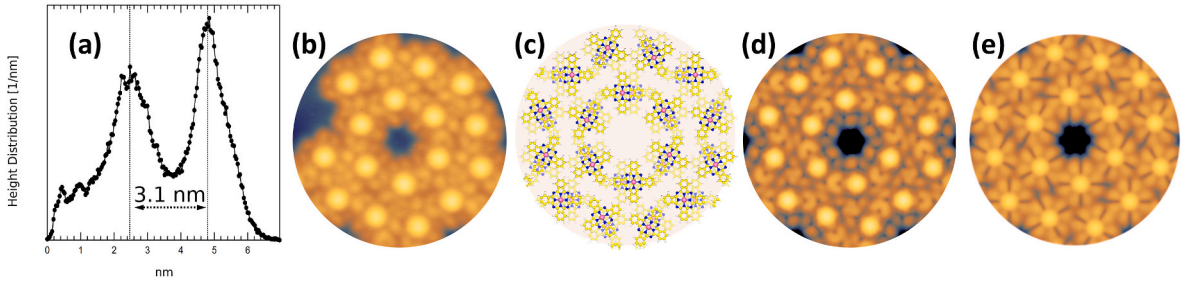

Fig. 8. FePc molecules self-assembled in a locally ordered hexagonal pattern around the "dot" site (oxygen vacancy) of the $Al_2O_3/Ni_3Al(111)$ support taken in a multilayer region. From the left to the right: (a) height distribution; (b) experimental STM image; (c) stick-and-ball model with a face-to-face stacking and optimized positions obtained by DFT; (d) simulated STM image for the face-to-face stacking; (e) simulated STM for the face-to-back stacking. The bias in the STM images is +2 V.

coverage is reached), in the case of a multilayer structure the chirality is not random but rather alternates between one layer and another.

CRediT authorship contribution statement

Fatema Mohamed: Writing – review & editing, Visualization, Software, Investigation, Data curation. **Manuel Corva:** Writing – review & editing, Validation, Investigation, Formal analysis, Data curation. **Erika Tomsič:** Visualization, Investigation, Data curation. **Zhijing Feng:** Visualization, Validation, Methodology, Investigation, Formal analysis, Data curation. **Tomáš Skála:** Writing – review & editing, Validation, Methodology, Investigation, Formal analysis, Data curation. **Giovanni Comelli:** Writing – review & editing, Validation, Supervision, Resources, Methodology, Funding acquisition, Conceptualization. **Nicola Seriani:** Writing – review & editing, Validation, Software, Methodology. **Erik Vesselli:** Writing – review & editing, Writing – original draft, Validation, Supervision, Resources, Methodology, Funding acquisition, Conceptualization. **Maria Peressi:** Writing – review & editing, Writing –

original draft, Validation, Supervision, Resources, Methodology, Investigation, Funding acquisition, Conceptualization.

Declaration of competing interest

The authors declare the following financial interests/personal relationships which may be considered as potential competing interests: Manuel Corva, Erika Tomsič, Zhijing Feng, Tomáš Skála, Giovanni Comelli and Erik Vesselli report access to the Materials Science beamline at Elettra was provided by Central European Research Infrastructure Consortium. Fatema Mohamed, Nicola Seriani, Maria Peressi report access to computational resources was provided by CINECA Supercomputing Center. If there are other authors, they declare that they have no known competing financial interests or personal relationships that could have appeared to influence the work reported in this paper.

Acknowledgments

The authors acknowledge the CERIC−ERIC consortium for access to the Materials Science beamline at Elettra. Computational resources have been obtained from the CINECA Supercomputing Center (Italy) through the ISCRA initiative and the agreement with the University of Trieste.

Data availability

Data will be made available on request.

References

[1] A.B.P. Lever, The phthalocyanines, Adv. Inorg. Chem. Radiochem. 7 (1965) 27, https://doi.org/10.1016/S0065-2792(08)60314-3.
[2] M.K. Engel, *Single-Crystal and solid-state molecular Structures of phthalocyanine complexes*, report kawamura inst, Chem. Res. 8 (1997) 11–54.
[3] J.M. Berg, J.L. Tymoczko, L. Stryer, Biochemistry, fifth ed., W.H. Freeman Publishing, New York, NY, U. S. A., 2002.
[4] X.F. Yang, A. Wang, B. Qiao, J. Li, J. Liu, T. Zhang, Single-atom catalysts: a new frontier in heterogeneous catalysis, Acc. Chem. Res. 46 (2013) 1740–1748, https://doi.org/10.1021/ar300361m.
[5] X.F. Chen, J.M. Yan, Q. Jiang, Single layer of polymeric metal–phthalocyanine: promising substrate to realize single Pt atom catalyst with uniform distribution, J. Phys. Chem. C 118 (4) (2014) 2122–2128, https://doi.org/10.1021/jp411183h.
[6] A.B. Sorokin, Phthalocyanine metal complexes in catalysis, Chem. Rev. 113 (2013) 8152–8191, https://doi.org/10.1021/cr4000072.
[7] J. Blochwitz, M. Pfeiffer, T. Fritz, K. Leo, Low voltage organic light emitting diodes featuring doped phthalocyanine as hole transport material, Appl. Phys. Lett. 73 (1998) 729–731, https://doi.org/10.1063/1.121982.
[8] G. Bottari, G. de la Torre, D.M. Guldi, T. Torres, Covalent and noncovalent Phthalocyanine−Carbon nanostructure systems: synthesis, photoinduced electron transfer, and application to molecular photovoltaics, Chem. Rev. 110 (2010) 6768–6816, https://doi.org/10.1021/cr900254z.
[9] W.R. Cao, J.G. Xue, Recent progress in organic photovoltaics: device architecture and optical design, Energy Environ. Sci. 7 (2014) 2123–2144, https://doi.org/10.1039/C4EE00260A.
[10] A.W. Hains, Z.Q. Liang, M.A. Woodhouse, B.A. Gregg, Molecular semiconductors in organic photovoltaic cells, Chem. Rev. 110 (2010) 6689–6735, https://doi.org/10.1021/cr9002984.
[11] M. Ince, J.H. Yum, Y. Kim, S. Mathew, M. Grätzel, T. Torres, M.K. Nazeeruddin, Molecular engineering of phthalocyanine sensitizers for dye-sensitized solar cells, J. Phys. Chem. C 118 (2014) 17166–17170, https://doi.org/10.1021/jp502447y.
[12] C.D. Dimitrakopoulos, P.R.L. Malenfant, Organic thin film transistors for large area electronics, Adv. Mater. 14 (2002) 99–117, https://doi.org/10.1002/1521-4095(20020116)14:2%3C99::AID-ADMA99%3E3.0.CO;2-9.
[13] M. Bevilacqua, J. Filippi, A. Lavacchi, A. Marchionni, H.A. Miller, W. Oberhauser, E. Vesselli, F. Vizza, Energy savings in the conversion of CO2 to fuels using an electrolytic device, Energy Technol. 2 (2014) 522–525, https://doi.org/10.1002/ente.201402014.
[14] R. Burkitt, T.R. Whiffen, Eileen Hao Yu, Iron phthalocyanine and MnOx composite catalysts for microbial fuel cell applications, Appl. Catal. B Environ. 181 (2016) 279–288, https://doi.org/10.1016/j.apcatb.2015.07.010.
[15] M. Corva, F. Mohamed, E. Tomsic, M. Rinaldi, C. Cepek, N. Seriani, M. Peressi, E. Vesselli, Learning from nature: charge transfer and carbon dioxide activation at single, biomimetic Fe sites in tetrapyrroles on graphene, J. Phys. Chem. C 123 (6) (2019) 3916–3922, https://doi.org/10.1021/acs.jpcc.8b11871.
[16] Y. Ren, J. Wang, M. Zhang, Y. Wang, Y. Cao, Dong Ha Kim, Zhiqun Lin, Locally ordered single-atom catalysts for electrocatalysis, Angew. Chem. Int. Ed. 63 (2024) e202315003, https://doi.org/10.1002/anie.202315003.
[17] P.S. Deimel, R.M. Bababrik, B. Wang, P.J. Blowey, L.A. Rochford, P.K. Thakur, Tien-Lin Lee, M.-L. Bocquet, J.V. Barth, D.P. Woodruff, D.A. Duncan, F. Allegretti, Direct quantitative identification of the "surface trans-effect", Chem. Sci. 7 (2016) 5647–5656, https://doi.org/10.1039/C6SC01677D.
[18] W. Hieringer, K. Flechtner, A. Kretschmann, K. Seufert, W. Auwärter, J.V. Barth, A. Görling, H.-P. Steinrück, J.M. Gottfried, The surface trans effect: influence of axial ligands on the surface chemical bonds of adsorbed metalloporphyrins, J. Am. Chem. Soc. 133 (2011) 6206–6222, https://doi.org/10.1021/ja1093502.
[19] M. Gottfried, H. Marbach, Surface-confined coordination chemistry with porphyrins and phthalocyanines: aspects of formation, electronic structure, and reactivity, Z. Phys. Chem. (Leipz.) 223 (2009) 53–74, https://doi.org/10.1524/zpch.2009.6024.
[20] Z.H. Cheng, L. Gao, Z.T. Deng, N. Jiang, Q. Liu, D.X. Shi, S.X. Du, H.M. Guo, H.-J. Gao, Adsorption behavior of iron phthalocyanine on Au(111) surface at submonolayer coverage, J. Phys. Chem. C 111 (2007) 9240–9244, https://doi.org/10.1021/jp070388l.
[21] Lu Xing, K.W. Hipps, Scanning tunneling microscopy of metal phthalocyanines: d^6 and d^8 cases, J. Phys. Chem. B 101 (27) (1997) 5391–5396, https://doi.org/10.1021/jp9707448.
[22] Z. Hu, B. Li, A. Zhao, J. Yang, J.G. Hou, Electronic and magnetic properties of metal phthalocyanines on Au(111) surface: a first-principles study, J. Phys. Chem. C 112 (35) (2008) 13650–13655, https://doi.org/10.1021/jp8043048.
[23] Y. Bai, F. Buchner, M.T. Wendahl, I. Kellner, A. Bayer, H.-P. Steinrück, H. Marbach, J.M. Gottfried, Direct Metalation of a Phthalocyanine Monolayer on Ag(111) with Coadsorbed Iron Atoms, J. Phys. Chem. C 112 (15) (2008) 6087–6092, https://doi.org/10.1021/jp711122w.
[24] K. Manandhar, K.T. Park, S. Ma, J. Hrbek, Heteroepitaxial thin film of iron phthalocyanine on Ag(111), Surf. Sci. 603 (4) (2009) 636–640, https://doi.org/10.1016/j.susc.2008.12.031.
[25] M. Casarin, M. Di Marino, D. Forrer, M. Sambi, F. Sedona, E. Tondello, A. Vittadini, V. Barone, M. Pavone, Coverage-dependent architectures of iron phthalocyanine on Ag(110): a comprehensive STM/DFT study, J. Phys. Chem. C 114 (5) (2010) 2144–2153, https://doi.org/10.1021/jp904260p.
[26] P. Gargiani, M. Angelucci, C. Mariani, M.G. Betti, Metal-phthalocyanine chains on the Au(110) surface: Interaction states versus d-metal states occupancy, Phys. Rev. B 81 (2010) 085412, https://doi.org/10.1103/PhysRevB.81.085412.
[27] T.G. Gopakumar, T. Brumme, J. Kröger, C. Toher, G. Cuniberti, R. Berndt, J. Phys. Chem. C 115 (24) (2011) 12173–12179, https://doi.org/10.1021/jp302233e.
[28] Y.H. Jiang, W.D. Xiao, L.W. Liu, L.Z. Zhang, J.C. Lian, K. Yang, S.X. Du, H.-J. Gao, Self-assembly of metal phthalocyanines on Pb(111) and Au(111) surfaces at submonolayer coverage, J. Phys. Chem. C 115 (44) (2011) 21750–21754, https://doi.org/10.1021/jp203462f.
[29] Y.Y. Zhang, S.X. Du, H.-J. Gao, Binding configuration, electronic structure, and magnetic properties of metal phthalocyanines on a Au(111) surface studied with ab initio calculations, Phys. Rev. B 84 (2011) 125446, https://doi.org/10.1103/PhysRevB.84.125446.
[30] A. Mugarza, R. Robles, C. Krull, R. Korytár, N. Lorente, P. Gambardella, Electronic and magnetic properties of molecule-metal interfaces: transition-metal phthalocyanines adsorbed on Ag(100), Phys. Rev. B 85 (2012) 155437, https://doi.org/10.1103/PhysRevB.85.155437.
[31] F. Petraki, H. Peisert, U. Aygül, F. Latteyer, J. Uihlein, A. Vollmer, T. Chassé, Electronic Structure of FePc and Interface Properties on Ag(111) and Au(100), J. Phys. Chem. C 116 (20) (2012) 11110–11116, https://doi.org/10.1021/jp302233e.
[32] A. Lehnert, A. Krupski, S. Degen, K. Franke, R. Decker, S. Rusponi, M. Kralj, C. Becker, H. Brune, K. Wandelt, *Nucleation of ordered Fe islands on Al_2O_3/Ni_3Al (111)*, Surf. Sci. 600 (2006) 1804–1808, https://doi.org/10.1016/j.susc.2006.02.013.
[33] J. Olmos-Asar, E. Vesselli, A. Baldereschi, M. Peressi, *Self-seeded nucleation of Cu nanoclusters on $Al_2O_3/Ni_3Al(111)$: an ab-initio investigation*, Phys. Chem. Chem. Phys. 16 (2014) 23134–23142, https://doi.org/10.1039/C4CP03271C.
[34] J. Olmos-Asar, E. Vesselli, A. Baldereschi, M. Peressi, *Towards optimal seeding for the synthesis of ordered nanoparticle arrays on alumina/$Ni_3Al(111)$*, Phys. Chem. Chem. Phys. 17 (2015) 28154–28161, https://doi.org/10.1039/C5CP00304K.
[35] M. Moors, A. Krupski, S. Degen, M. Kralj, C. Becker, K. Wandelt, *Scanning tunneling microscopy and spectroscopy investigations of copper phthalocyanine adsorbed on $Al_2O_3/Ni_3Al(111)$*, Appl. Surf. Sci. 254 (2008) 4251–4257, https://doi.org/10.1016/j.apsusc.2008.01.029.
[36] M. Corva, F. Mohamed, E. Tomsic, Z. Feng, T. Skala, G. Comelli, N. Seriani, M. Peressi, E. Vesselli, Substrate- to laterally-driven self-assembly steered by Cu nanoclusters: the case of FePcs on an ultrathin alumina film, ACS Nano 12 (11) (2018) 10755–10763, https://doi.org/10.1021/acsnano.8b05992.
[37] E. Vesselli, A. Baraldi, S. Lizzit, G. Comelli, Large interlayer relaxation at a metal-oxide interface: the case of a supported ultrathin alumina film, Phys. Rev. Lett. 105 (2010) 046102, https://doi.org/10.1103/PhysRevLett.105.046102.
[38] P. Giannozzi, S. Baroni, N. Bonini, M. Calandra, R. Car, C. Cavazzoni, D. Ceresoli, G.L. Chiarotti, M. Cococcioni, I. Dabo, A. Dal Corso, S. Fabris, G. Fratesi, S. de Gironcoli, R. Gebauer, U. Gerstmann, C. Gougoussis, A. Kokalj, M. Lazzeri, L. Martin-Samos, N. Marzari, F. Mauri, R. Mazzarello, S. Paolini, A. Pasquarello, L. Paulatto, C. Sbraccia, S. Scandolo, G. Sclauzero, A.P. Seitsonen, A. Smogunov, P. Umari, R.M. Wentzcovitch, Quantum ESPRESSO: a modular and open-source software project for quantum simulations of materials, J. Phys. Condens. Matter 21 (2009) 395502, https://doi.org/10.1088/0953-8984/21/39/395502.
[39] D. Vanderbilt, Soft self-consistent pseudopotentials in a generalized eigenvalue formalism, Physical Review B, Condensed Matter 41 (1990) 7892–7895, https://doi.org/10.1103/PhysRevB.41.7892.

[40] J.P. Perdew, K. Burke, M. Ernzerhof, Generalized gradient approximation made simple, Phys. Rev. Lett. 77 (1996) 3865–3868, https://doi.org/10.1103/PhysRevLett.77.3865. Erratum Phys. Rev. Lett. 78, 1396 (1997).
[41] S. Grimme, Semiempirical GGA-type density functional constructed with a long-range dispersion correction, J. Comput. Chem. 27 (2006) 1787–1799, https://doi.org/10.1002/jcc.20495.
[42] M. Schmid, G. Kresse, A. Buchsbaum, E. Napetschnig, S. Gritschneder, M. Reichling, P. Varga, *Nanotemplate with holes: ultrathin Alumina on $Ni_3Al(111)$*, Phys. Rev. Lett. 99 (2007) 196104, https://doi.org/10.1103/PhysRevLett.99.196104.
[43] J.N. Andersen, D. Hennig, E. Lundgren, M. Methfessel, R. Nyholm, M. Scheffler, Surface core-level shifts of some 4d-metal single-crystal surfaces: Experiments and ab initio calculations, Phys. Rev. B 50 (1994) 17525, https://doi.org/10.1103/PhysRevB.50.17525.
[44] J. Tersoff, D.R. Hamann, Theory of the scanning tunneling microscope, Phys. Rev. B 31 (1985) 805, https://doi.org/10.1103/PhysRevB.31.805.
[45] M. Cococcioni, S. de Gironcoli, Linear response approach to the calculation of the effective interaction parameters in the LDA+U method, Phys. Rev. B 71 (2005) 035105, https://doi.org/10.1103/PhysRevB.71.035105.
[46] S. Gritschneder, C. Becker, K. Wandelt, M. Reichling, Disorder or complexity? Understanding a nanoscale template structure on alumina, J. Am. Chem. Soc. 129 (2007) 4925–4928, https://doi.org/10.1021/ja065118f.